Cell wall thickness has phylogenetically consistent effects on photosynthetic nitrogen-use efficiency of terrestrial plants: a meta-analysis

Dan-dan Liu[1†], Tiina Tosens[2], Dong-liang Xiong[3], Marc Carriquí[4], You-cai Xiong[1], Wei Xue[1*,†]

[1]College of Ecology, State Key Laboratory of Grassland Agroecosystems, Lanzhou University, Lanzhou 730000, China

[2]Institute of Agricultural and Environmental Sciences, Estonian University of Life Sciences, Kreutzwaldi, Tartu 51014, Estonia

[3]National Key Laboratory of Crop Genetic Improvement, Hubei Hongshan Laboratory, MOA Key Laboratory of Crop Ecophysiology and Farming System in the Middle Reaches of the Yangtze River, Huazhong Agricultural University, Wuhan 430070, China

[4]Research Group on Plant Biology under Mediterranean Conditions, Institut d'Investigacions Agroambientals i d'Economia de l'Aigua (INAGEA) – Universitat de les Illes Balears (UIB), Ctra Valldemossa Km 7.5., 07122, Illes Balears, Spain

*Corresponding author: Wei Xue. E-mail: xuewei@lzu.edu.cn, Tel: 0931-8915950

†These authors contributed equally to this work

Current address for Wei Xue: Lanzhou University, No.222 Tianshui South Road, Lanzhou, China

Running title: Cell wall thickness constrains PNUE of land plants

Abstract Leaf photosynthetic nitrogen-use efficiency (PNUE) diversified significantly among C_3 species. However, morpho-physiological mechanisms and interrelationships forming PNUE remain unclear on the evolutionary time scale. In this study, we compiled a novel extensive matrix of morpho-anatomical and physiological traits of leaf in 679 C_3 species ranging from bryophytes to angiosperms to understand the intricacy of interrelationships underlying the variations in PNUE. We found that LMA, mesophyll cell wall thickness (T_{cwm}), Rubisco N allocation fraction (P_R), and mesophyll conductance (g_m) together interpreted 83% of variations in PNUE, with P_R and g_m accounting for 65% of those variations. However, the P_R effects were species-dependent on g_m; that is, the contribution of P_R on PNUE was extensively significant in high-g_m species in comparison to low-g_m species. Standard major analysis (SMA) and path analysis suggested a weak correlation between PNUE and LMA, whereas the SMA correlation for PNUE–T_{cwm} was strong. The P_R was inversely proportional to T_{cwm}, which was similar to the relationship between g_m and T_{cwm} (p-value < 0.01), so that the internal CO_2 drawdown from intercellular airspace to carboxylaton sites was relatively conservative over a wide range of T_{cwm}. Collectively, the coordination of changes in P_R and g_m connecting T_{cwm} suggested the complex physiological mechanisms mediated by T_{cwm} modulating PNUE across contrasting plant groups.

Keywords: Photosynthetic nitrogen-use efficiency; Nitrogen allocation; Mesophyll conductance; Cell wall thickness; Leaf mass per area

Introduction

Trait-based ecology is an emerging discipline, aiming to predict functional diversity of population, communities, and ecosystems using the generalizable, functional properties of individual organisms (De Bello *et al*., 2021). Leaf photosynthetic nitrogen-use efficiency (PNUE), defined as the ratio of light-saturated photosynthesis to leaf nitrogen content, is a fundamental process of the leaf economics spectrum (LES) (Wright *et al*., 2005). Significant variations were observed in the PNUE economic trait. In spermatophyte, there is a correlation between PNUE and leaf mass per area (LMA); species with high LMA almost invariably have low PNUE (Reich *et al*., 1998; Wright *et al*., 2005; Onoda *et al*., 2017). The LMA, as a complex leaf morphologic trait, could not explain inter-specific PNUE variations (Shipley *et al*., 2006; Warren and Adams, 2006; Hidaka and Kitayama, 2009; Onoda *et al*., 2017; Flexas and Carriquí, 2020; Luo *et al*., 2021). The morpho-physiological mechanisms and interrelationships underlying the PNUE are attracting ever-increasing attention owning to the ecological significance of the inter-specific variations of PNUE in relation to relative growth rate and crop yield or for the sake of realistic ecosystem modeling (Poorter *et al*., 1990; Garnier *et al*., 1995; Reich *et al*., 1998; Oguchi *et al*., 2016; Yin *et al*., 2019).

Previous studies demonstrated that variations in PNUE resulted from interactive mechanisms of several physiological and anatomical traits of foliage (Hikosaka, 2004, 2010; Wright *et al*., 2005; Onoda *et al*., 2017; Flexas and Carriquí, 2020). Specifically, nitrogen allocation into photosynthetic apparatus and mesophyll conductance for internal CO_2 diffusion (g_m) were important. In spermatophyte, experimental studies observed an inverse relationship between LMA and the fraction of nitrogen allocated to photosynthetic proteins. With increasing LMA in ten dicotyledonous species, the photosynthetic N allocation fraction decreased from 50% to 38%, with a significant decrease in the Rubisco N allocation fraction (P_R) (Poorter and Evans, 1998). Hikosaka *et al*. (1998) analyzed an annual herb and an evergreen tree, reporting a higher P_R of 23.2% in the low-LMA herb in comparison to the high-LMA tree. Similar results were also observed in other studies where the high-LMA species and genotypes exhibited a reduced P_R (Warren and Adams, 2000; Ripullone *et al*., 2003; Onoda *et al*., 2004; Pons and Westbeek, 2004; Takashima *et al*., 2004; Onoda *et al*., 2017; Gvozdevaite *et al*., 2018; Lei *et al*., 2021a). A meta-analysis in spermatophyte performed by Onoda *et al*. (2017) attributed the negative relationship

between PNUE and LMA to the trade-off mechanisms between photosynthesis and structural persistence (hereinafter referred to LMA-mediated function-structure tradeoff in spermatophyte), which means that species at the high-end of the LMA axis were more likely to preserve a greater fraction of leaf nitrogen in structural tissues, resulting in lower P_R and PNUE. The PNUE variation from the low-end LMA axis to the high-end was associated with increased N investments in structural tissue. Recently, a study that quantified the negative P_R–LMA relationship in spermatophyta has supported it (Luo *et al*., 2021).

An inevitable result of the construction cost for structural tissues is a decrease in g_m (Onoda *et al*., 2017; Flexas and Carriquí, 2020), with a tendency for g_m to decline from the low- to the high-end of the LMA axis in spermatophyta. In ferns and mosses, the observed variations in PNUE were strongly associated with g_m (Tosens *et al*., 2016; Carriquí *et al*., 2019). Ferns and mosses with similar LMA as seed plants clustering at the low-end of the LMA axis exhibited substantially lower g_m and PNUE (Carriquí *et al*., 2015; Tosens *et al*., 2016; Zhu *et al*., 2016; Z. Wang *et al*., 2017), which indeed was in contradiction to the negative PNUE–LMA pattern on which the LMA-based function-structure tradeoffs were dependent. In contrast to the critical roles of g_m in PNUE in mosses and ferns, several studies in seed plants discovered that g_m did not contribute to PNUE variations in 11 evergreen tropical and temperate species that differed in LMA (Bahar *et al*., 2018) as well as in 26 wild and 31 domesticated cotton genotypes with significant variations in LMA (Lei *et al*., 2021b). It suggested that the LMA-based function-structure tradeoff paradigm developed by Onoda *et al*. (2017) might have a limited capability of addressing the underpinnings of PNUE variations across the phylogeny of land plant.

Bryophytes and pteridophytes are significant from an evolutionary perspective owning to their pioneering positions in the land transition of photosynthetic life; they are currently attracting considerable attention among researchers owning to their great potential in biotechnology and bioindication (Preston and Hill, 1999; Popper and Fry, 2003; Wang *et al*., 2013; Gago *et al*., 2019; Flexas and Carriquí, 2020). Concerning the above mentioned disputes, earlier studies attributed diversions of paired-trait relationships among major plant groups to leaf habits or height-based economics spectrum (Zhao *et al*., 2017; Li *et al*., 2022) or microhabitat acclimations (Keenan and Niinemets, 2016; Anderegg *et al*., 2018) or unknown fundamental difference (Waite and Sack, 2009; Z. Wang *et al*., 2017). Until now, LMA has not been well understood

in terms of its role in PNUE variations, its correlations with g_m and P_R, as well as the mechanisms involved in g_m and P_R functioning across major plant groups and phylogenetic interrelationships.

The g_m is a highly complex trait that mediates liquid phase diffusion and is highly sensitive to leaf anatomy and biochemical traits (e.g., effective porosity of the cell wall-p_i, the CO_2 permeability of membranes, carbonic anhydrase activity, etc.) (Evans *et al*., 2009; Kaldenhoff, 2012; Tosens *et al*., 2012; Han *et al*., 2018; Gago *et al*., 2019; Carriquí *et al*., 2020; Evans, 2021; Flexas *et al*., 2021), which consolidate attempts to scale PNUE with g_m (Warren and Adams, 2006). Pleiotropic compensatory changes (e.g., one advantageous factor compensates for another drawback) might exert distinct roles when comparing PNUE across a few species or species occupying the same habitat in which resource use strategies tend to converge (Evans *et al*., 2009; Anderegg *et al*., 2018; Lei *et al*., 2021b; Nadal *et al*., 2021). In this study, a global extensive database was compiled, including leaf morphological, anatomical, and physiological traits of terrestrial C_3 species ranging from bryophytes to angiosperm. Data in C_4 species that have distinct photosynthetic mechanisms than C_3 species were not the major concern in this study. Data analysis and presentation in *Results* section were performed within major taxonomic group (i.e., bryophytes, pteridophytes, gymnosperm, and angiosperm) and across taxonomic groups, helping clarify the scales at which our results were applicable. Specifically, we aimed to address three questions as follows:

(1) What is the evolutionary pattern of PNUE from bryophytes to angiosperms? Are PNUE variations primarily associated with LMA across major taxonomic groups?

(2) What are the crucial morpho-anatomical traits in shaping PNUE variations across major taxonomic groups?

(3) What are the interrelationships between these important morpho-anatomical traits and PNUE across major taxonomic groups?

Results

The evolutionary pattern of PNUE and its relationship with LMA

Significant phylogenetic signals were observed for the LMA, PNUE, A_{mass}, N_m, V_{cmax}, J_{max}, P_R, g_m, DeltaC, and T_{cwm} (Table S1). Initially, we mapped the LMA phylogenetic pattern and its relationship with PNUE, A_{mass}, and N_m as LMA was considered an important factor influencing the PNUE economic trait in seed plants

(Hikosaka, 2004; Wright *et al*., 2005; Onoda *et al*., 2017). The mean of LMA cluster data largely increased from bryophytes to pteridophytes (TukeyHSD, p-value = 0.07) (Figure 1a). No significant differences were observed in mean LMA between pteridophytes and angiosperms (p-value = 0.27, Figure 1a). The mean LMA in gymnosperms was significantly higher in comparison to the other three phyla (p-value < 0.01). The mean PNUE values from the ANOVA revealed significant differences across the four phyla (Figure 1b), with the angiosperms having the highest PNUE values (p-value < 0.05) and the other three phyla having similar PNUE values (p-value > 0.1). Significantly, PNUE was lower in bryophytes at the same LMA as seed plants and marginally lower in pteridophytes (Figure 1c). The LES SMA regression (fit SMA model to all data in the four phyla) exhibited a low r^2 at 0.1 owning to a significant deviation of bryophytes data from the LES SMA regression line (Figure 1c, SMA ANOVA in intercept: p-value < 0.01). Improved performance in the LES SMA regression for A_{mass}–LMA was evident ($r^2 = 0.33$); whereas all A_{mass} values in bryophytes significantly deviated from the LES SMA regression line primarily owning to major differences in intercept (Figure 1d, SMA ANOVA in intercept: p-value < 0.01). The LES SMA regression line and the phylum SMA regression lines (fit SMA model to data of each phylum) for the N_m–LMA relationship were in close proximity to one another (Figure 1e), demonstrating significantly higher $r^2 = 0.53$. Inequality in the number of sampled species among the four phyla did not distort the SMA correlation results. It was suggested that variations in PNUE through plant phylogeny were weakly associated with LMA primarily owning to large discrepancies in slope and intercept of the A_{mass}–LMA relationship among major taxonomic groups.

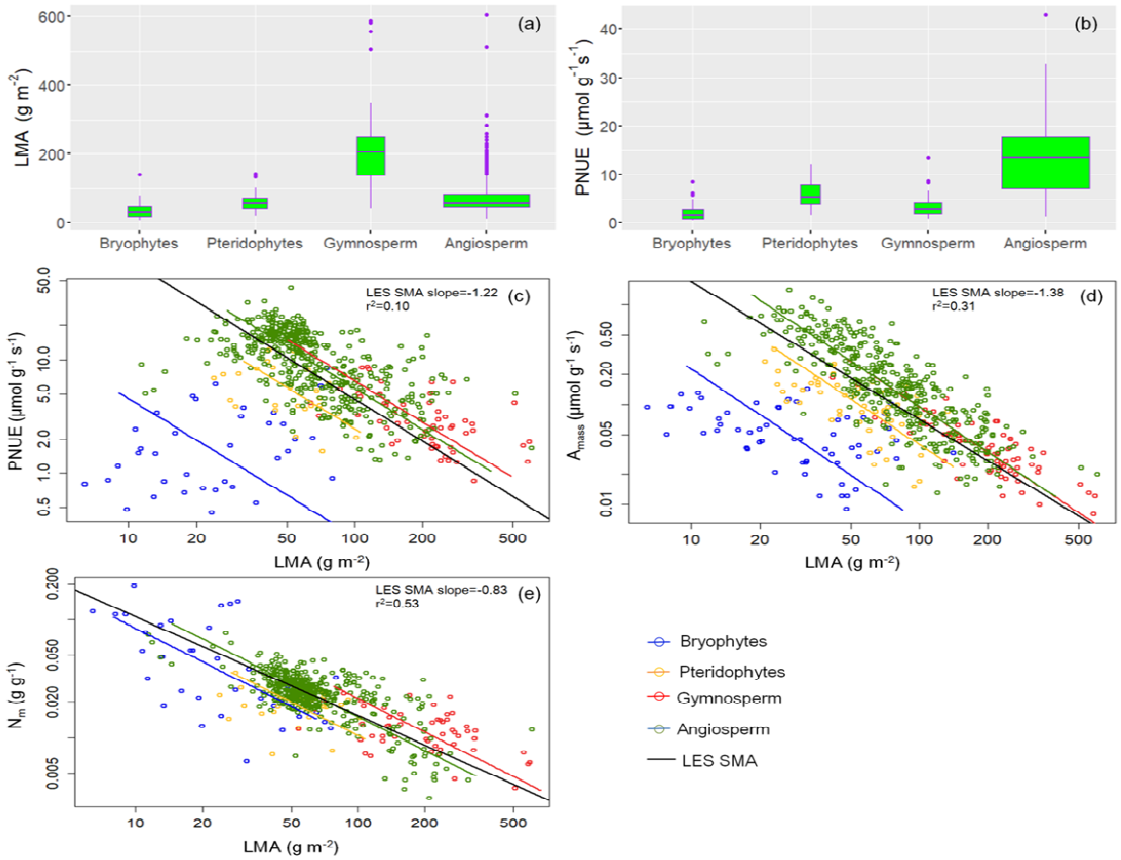

Figure 1. The phylogenetic patterns of leaf mass per area (LMA), (a) and photosynthetic N-use efficiency (PNUE), (b) as well as the paired-trait relationships between PNUE, mass-based photosynthesis capacity (A_{mass}), leaf nitrogen content per leaf mass (N_m), and LMA. (c) PNUE–LMA, (d) A_{mass}–LMA, and (e) N_m–LMA. The black line represents the regression of standard major analysis (SMA) fit to all data in the four phyla (LES SMA), and the other lines represent regressions of SMA fit to all data of each phylum. The r^2 and slope values were elucidated for the LES SMA regression. The boxes were drawn with widths proportional to the square-roots of the number of observations in each phylum. The same symbol legends for bryophytes, pteridophytes, gymnosperms, and angiosperms as in Figure 1 were used in other figures unless otherwise indicated.

Effects of photosynthetic nitrogen allocation and g_m on photosynthesis and PNUE variations

Although no significant correlation was observed for PNUE–N_m (LES SMA r^2 = 0.002, p-value = 0.32), the LES SMA fit for PNUE–A_{mass} exhibited r^2 as high as 0.58 (Figure S1), indicating that PNUE changing pattern along the LMA axis was strongly shaped by A_{mass}. Therefore, quantitative correlations between important physiological traits and A_{mass} were explored in this section. A positive LES SMA regression line for the A_{mass}–V_{cmax} relationship exhibited r^2 = 0.68, which overlapped the four phylum regression lines efficiently (Figure 2a, SMA ANOVA in slope: p-value = 0.07). A

closer correlation of the LES SMA regression fit to A_{mass}–g_m was evident with r^2 at 0.74, showing no significant differences against phylum regression lines (Figure 2b, SMA ANOVA in slope: p-value = 0.9). The V_{cmax} was closely related to J_{max} with r^2 as high as 0.89 (Figure 2c), close to four phylum regression lines (SMA ANOVA in slope: p-value = 0.04). The relationship between g_m and V_{cmax} exhibited relatively weaker correlation strength in comparison to V_{cmax}–J_{max} (r^2 = 0.5, Figure 2d).

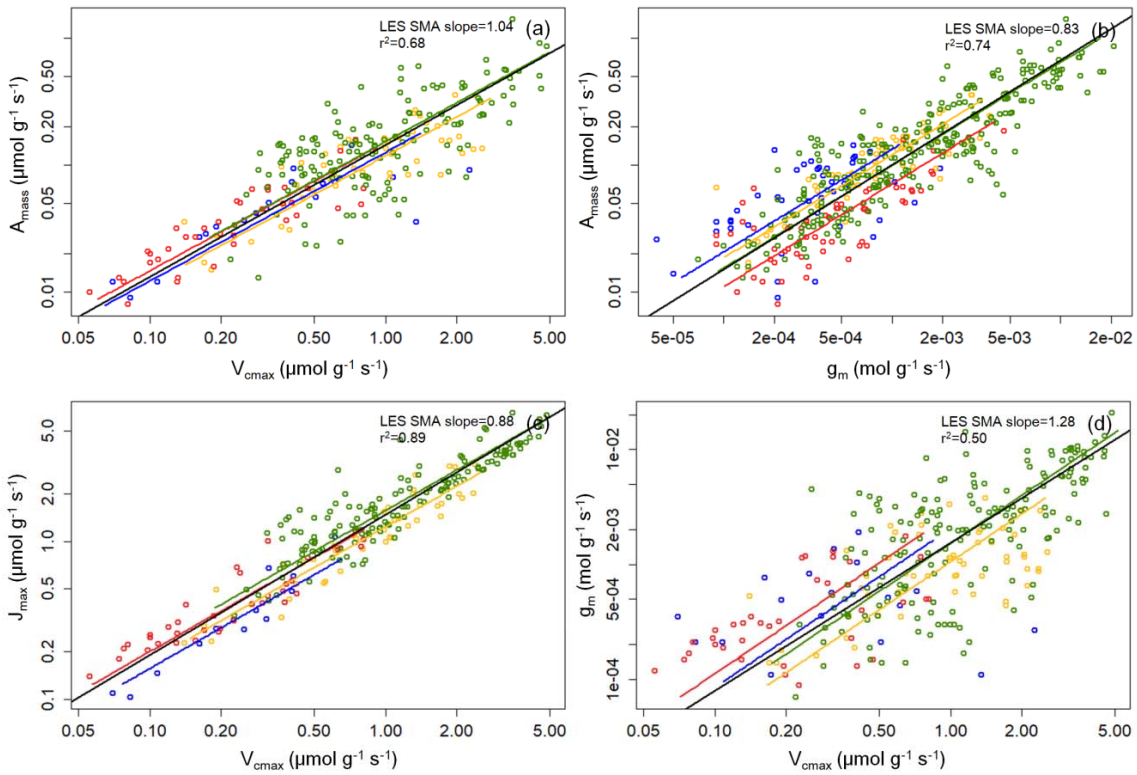

Figure 2. Paired-trait correaltions between the mass-based photosynthesis (A_{mass}), the mass-based maximum carboxylation rate (V_{cmax}), the mass-based mesophyll conductance (g_m), and the mass-based maximum electron transport rate (J_{max}). (a) A_{mass}–V_{cmax}, (b) A_{mass}–g_m, (c) V_{cmax}–J_{max}, and (d) g_m–V_{cmax}. The black line represents the regression of standard major analysis (SMA) fit to all data in the four phyla (LES SMA) and the other lines represents the regressions of SMA fit to all data of each phylum. The r^2 and slope values were elucidated for the LES SMA regression.

The A_{mass} was significantly regulated by V_{cmax} which was, in turn, related to P_R (LES SMA r^2 = 0.62). According to Onoda *et al*. (2017), DeltaC might be an important factor influencing PNUE variations in seed plants. Hence, PNUE relationships with P_R, g_m, and DeltaC were quantified in Figure 3. Across the four phyla, we observed substantial correlation strength between PNUE and P_R (r^2 = 0.45, Figure 3a). The PNUE–g_m correlation had a higher r^2 (0.52, Figure 3c) in comparison to P_R. According to path analysis, two traits explained approximately 65% of PNUE variations. Across the four phyla, there was no discernible correlation between PNUE

and DeltaC (r^2 = 0.04, Figure 3c). The r^2 value was considerably lower for the P_R–g_m relationship (r^2 = 0.20, Figure 3d), indicating a weak correlation between them.

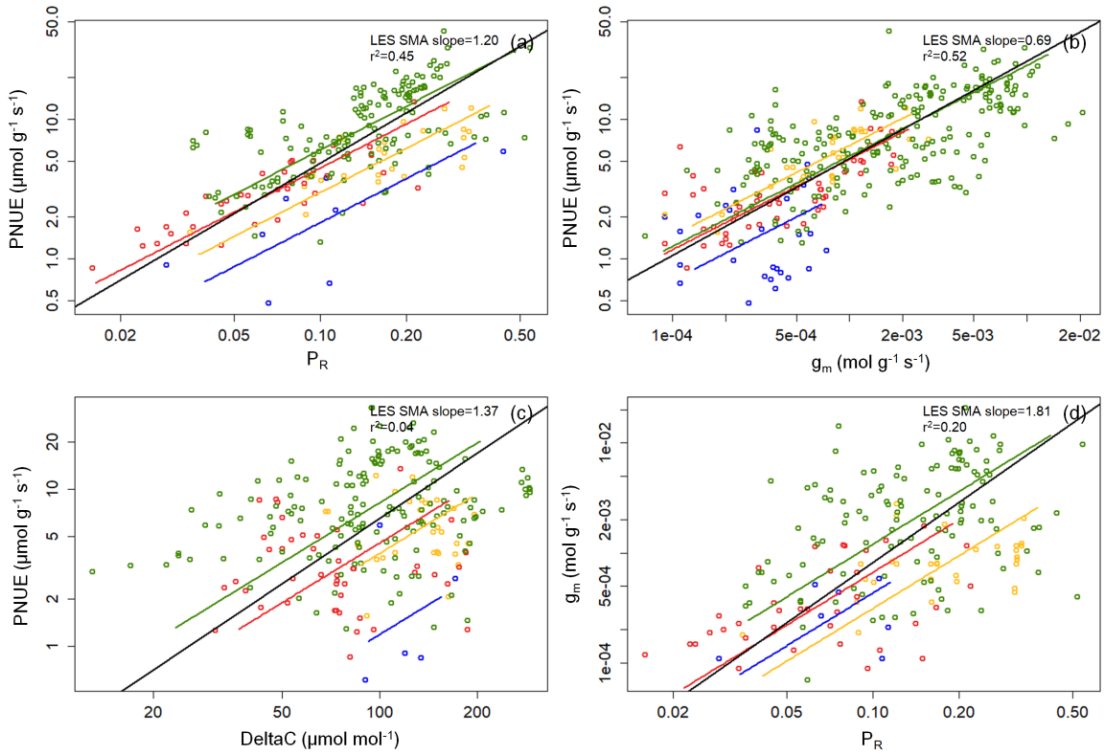

Figure 3. Paired-trait correlations between photosynthetic N-use efficiency (PNUE), allocation fraction of leaf nitrogen to Rubisco (P_R), mass-based mesophyll conductance (g_m), and internal CO_2 drawdown (DeltaC). (a) PNUE–P_R, (b) PNUE–g_m, (c) PNUE–DeltaC, (d) P_R–g_m. The black line represents the regression of standard major analysis (SMA) fit to all data in the four phyla (LES SMA) and the other lines represent the regressions of SMA fit to all data of each phylum. The r^2 and slope values were elucidated for the LES SMA regression.

The relative importance of P_R and g_m in determining PNUE is shown in Figure 4. The PNUE predictions corresponded to observations efficiently at both low- and high-g_m species assembles (Figure 4a). A close correspondence between PNUE predictions and observations was also noticed in most sampled species studied (Figure S2). The slope of the PNUE–P_R relationship was 57.58 in the high-g_m species assemble and 20.52 in the low-g_m species assemble. It indicated that for species with high g_m, a 0.1-unit increase in P_R contributed to a 5.8-unit increase in PNUE, while the increase in PNUE was only 2.1-unit in low-g_m species. An exponential decreasing tendency in l_m-l_b with g_m was observed in sampled species (Figure 4b). The l_m overweighed l_b in species with low g_m < 0.001 mol g^{-1} s^{-1} (approximately 0.08 mol m^{-2} s^{-1}), indicating stronger mesophyll limitation on photosynthesis; conversely, species with high g_m > 0.001 mol g^{-1} s^{-1} exhibited a stronger biochemical limitation on photosynthesis. These

results indicated a stronger limitation by g_m on PNUE for species with low g_m and a stronger limitation by P_R on PNUE for species with high g_m.

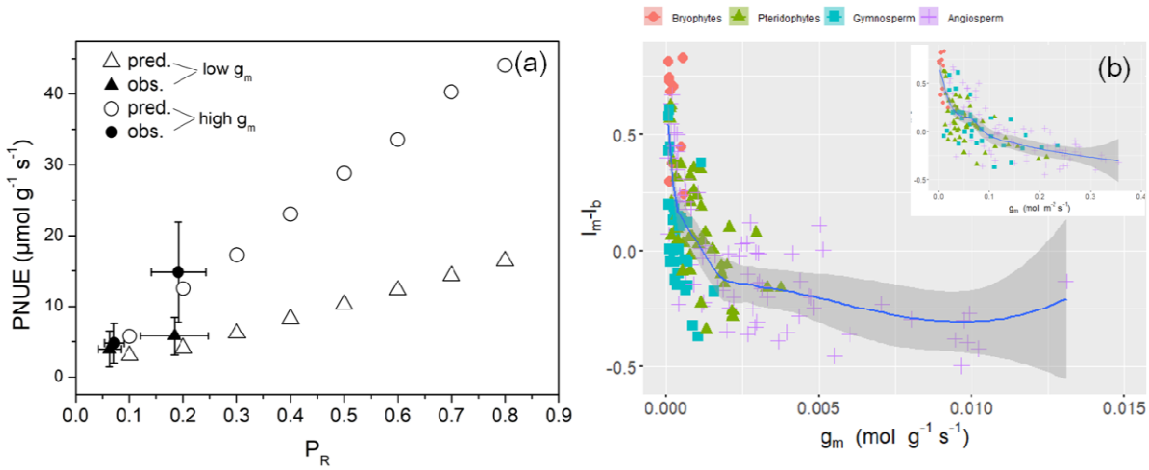

Figure 4. Model simulations and observations of photosynthetic N-use efficiency (PNUE) at a continuous series of Rubisco nitrogen allocation fraction (P_R) and at two assembles of mesophyll conductance (g_m), such as high and low ranges (circles and triangles, respectively) in subplot a. Subplot b demonstrates the relationship between l_m-l_b and mass-and area-based g_m. The high-g_m species assemble had a g_m range of 0.25–0.32 mol m^{-2} s^{-1}; whereas the low-g_m species assemble and 0.05–0.06 mol m^{-2} s^{-1}, corresponding to chloroplast CO_2 concentration (C_c) at approximately 100 and 230 μmol mol^{-1} under current atmospheric CO_2 conditions, respectively. pred.: predictions; obs.: observations; l_m-l_b: the difference between mesophyll conductance limitation and biochemical limitation.

Relationships between morpho-anatomical traits and P_R and g_m

Relationships between morpho-anatomical traits and P_R and g_m are illustrated in Figure 5. The P_R exhibited a weak correlation with LMA across the four phyla (r^2 = 0.19, Figure 5a) and the weak correlation was also observed between g_m and LMA (r^2 = 0.24, Figure 5b). Statistical findings in comparison between Onoda P_R chemical assay dataset and the P_R numerical calculations in spermatophyte exhibited no significant differences in SMA slope and intercept (p = 0.1, Figure S3), indicating that the incorporation of the P_R numerical calculations into Onoda P_R chemical assay dataset did not introduce systematic biases in trait correlation analysis, and the P_R mixture dataset was reliable. The four phyla exhibited a consistent relationship with high correlation strength for g_m and T_{cwm} (r^2 = 0.44, Figure 5c). The g_m in four phyla had the tendency to converge toward the Loess regression line (inset in Figure 5c). A rapid decline in g_m with T_{cwm} was observed, and g_m had the tendency to level off at higher T_{cwm}. A strong correlation was observed between g_m and the mass-based S_c (r^2

= 0.66, Figure 5d). No other anatomical traits revealed a significant correlation with g_m ($r^2 < 0.1$, Figures S4a–f). The P_R was inversely proportional to T_{cwm} with an average $r^2 = 0.30$ (Figure 5e). Although their correlation was much weaker ($r^2 = 0.14$, Figure 5f), the DeltaC increased with increasing T_{cwm}, indicating marginal effects of T_{cwm} on the internal CO_2 drawdown.

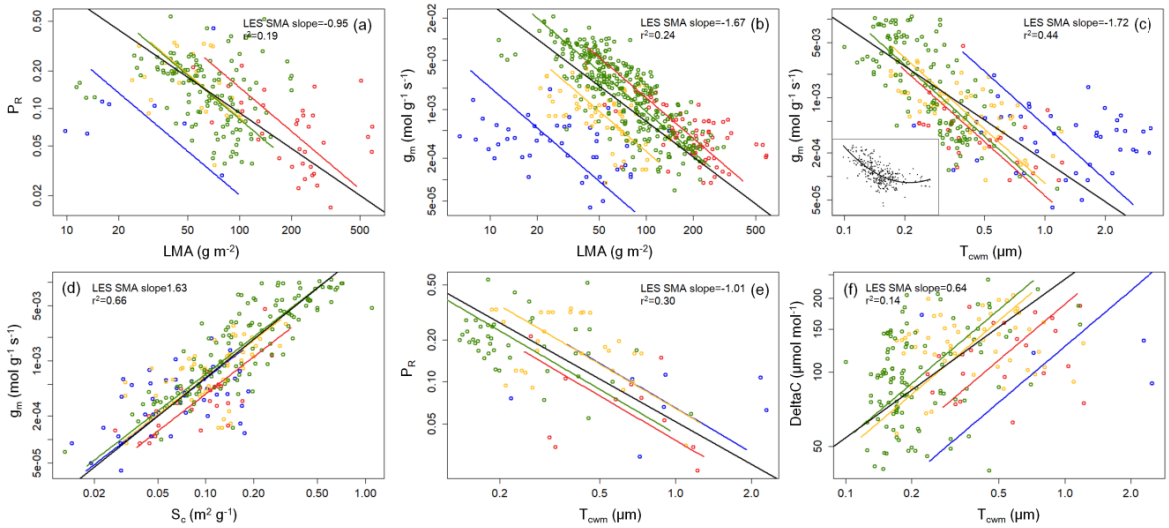

Figure 5. Paired-trait correlations between allocation fraction of leaf nitrogen to Rubisco (P_R), leaf mass per area (LMA), mesophyll conductance (g_m), mesophyll cell wall thickness (T_{cwm}), chloroplast surface exposed to intercellular airspace area per unit leaf mass (S_c), and internal CO_2 drawdown (DeltaC). (a) P_R–LMA, (b) g_m–LMA, (c) g_m–T_{cwm}, (d) g_m–S_c, (e) P_R–T_{cwm}, (f) DeltaC–T_{cwm}. The black line represents the regression of standard major analysis (SMA) fit to all data in the four phyla (LES SMA) and the other lines represent the regressions of SMA fit to all data of each phylum. The r^2 and slope values were elucidated for the LES SMA regression. The inset in subplot c exhibited the Loess model fit to the g_m–T_{cwm} correlation.

Path analysis for leaf morpho-anatomical and physiological traits and PNUE

According to path analysis for the SEM fit, the seven traits, such as g_m, P_R, LMA, T_{cwm}, mass-based S_c, C_i, and C_c together explained 88% of PNUE variations, while P_R and g_m interpreted 65% of PNUE variations (CFI = 1.0, SRMR = 0.02, p-value = 0.001, Figure 6a). The traits utilized for path analysis were chosen primarily according to the aforementioned paired-trait correlation analysis and Eqn. 3 parameters. The absolute value of path coefficient (Q) for T_{cwm}–g_m was 0.84, which was higher by 13.5% than in comparison to LMA–g_m. The S_c–g_m had a high $Q = 0.89$, confirming their positive correlation shown in Figure 5d. A higher Q value of 27.5% was found in the T_{cwm}–P_R in comparison to the LMA–P_R. The Q values for P_R–C_i or P_R–C_c were less than 0.3, which suggested minimal effects of leaf internal CO_2

concentration on P_R variations across species. The P_R and g_m exhibited direct and substantial effects on PNUE (Q > 0.45), while T_{cwm} and LMA exhibited direct and much weaker effects on PNUE (Q = 0.1 and 0.25, respectively). The phylogenic pattern of T_{cwm} across four phylum groups and the paired-trait correlation for PNUE–T_{cwm} are provided in Figures 6b and c. A trend of consistent decline in T_{cwm} from bryophytes to angiosperms was observed. The PNUE was negatively proportional to T_{cwm} with r^2 as high as 0.61, which was higher by five-fold in comparison to the PNUE–LMA relationship illustrated in Figure 1c. According to the findings, P_R and g_m variations across the four phyla and through plant phylogeny were primarily related to T_{cwm}. Effects of T_{cwm} on PNUE were achieved through its controls on P_R and g_m.

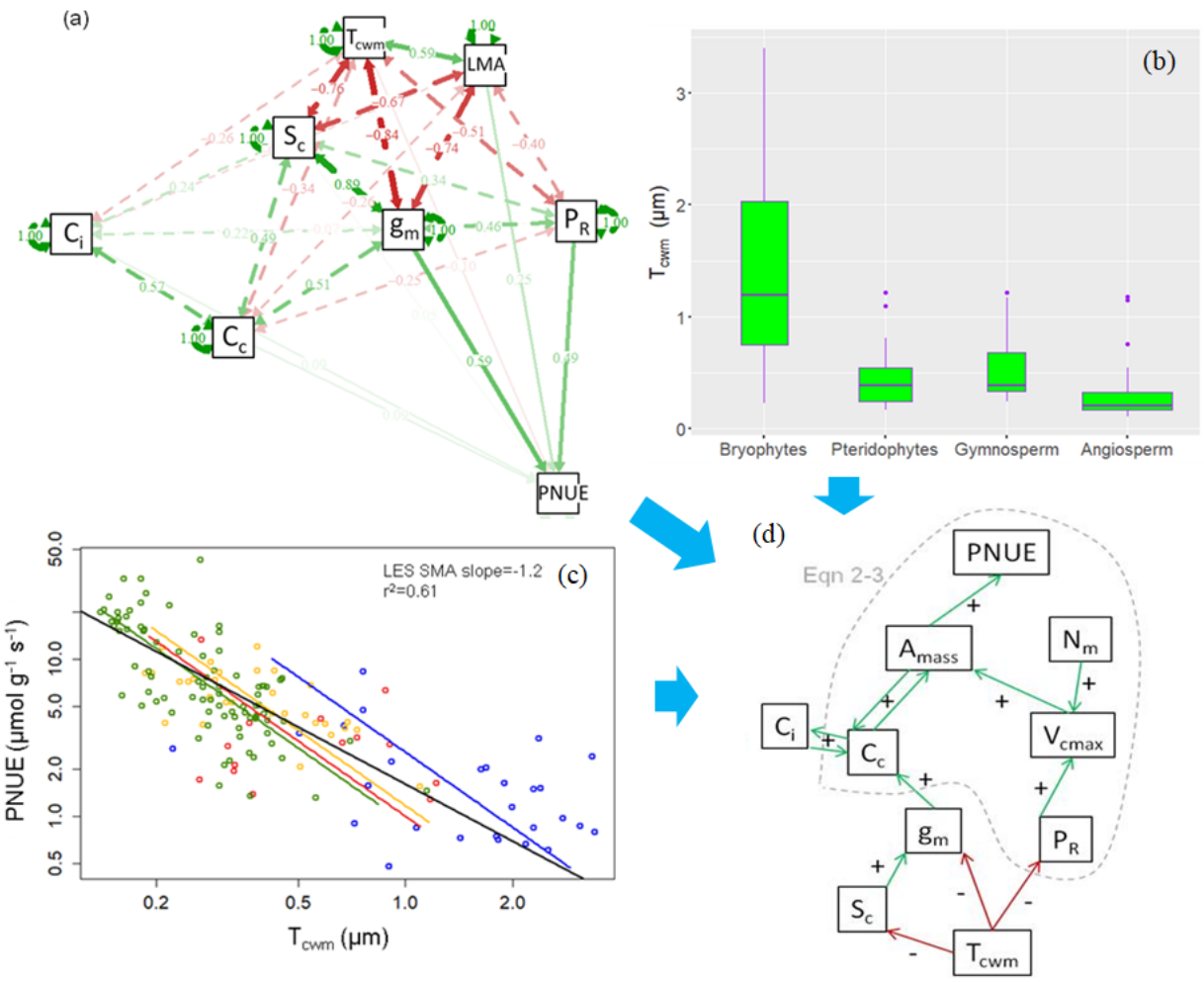

Figure 6. (a) The circle layout of the path diagram that indicates relationships and the causal direction between PNUE and morpho-physiological traits, (b) the phylogenetic patterns of mesophyll cell wall thickness (T_{cwm}), (c) the paired-trait correlation between photosynthetic-N use efficiency (PNUE) and T_{cwm}, and (d) the structural

diagram about T_{cwm}-mediated physiological mechanisms controlling PNUE variations. The path coefficient is represented by the arrow and value between each trait and PNUE in subplot a. The boxes were drawn with widths proportional to the square-roots of the number of observations in each phylum in subplot b. The black line represents the regression of standard major analysis (SMA) fit to all data in the four phyla (LES SMA) and the other lines represent the regressions of SMA fit to all data of each phylum in subplot c. The r^2 and slope values were elucidated for the LES SMA regression. Interrelationships between PNUE and leaf traits embedded by the gray dashed circle in subplot d were deduced from Eqn. 2 and 3. The "+" and "-" signs reflected positive and negative relations, respectively. P_R: allocation fraction of leaf nitrogen to Rubisco; LMA: leaf mass per area; g_m: mass-based mesophyll conductance; T_{cwm}: mesophyll cell wall thickness; S_c: chloroplast surface area exposed to intercellular airspace per unit leaf mass; C_i and C_c: leaf intercellular and chloroplastic CO_2 concentration, respectively.

Discussion

Thematic results with causal relationships between leaf functional traits and PNUE are illustrated in Figure 6d. According to Eqn. 2 and 3, A_{mass} is determined by C_c and V_{cmax}, which are in turn primarily related to C_i and g_m, P_R and N_m, respectively. An increase in N_m could contribute to V_{cmax} and, subsequently A_{mass}, while its contributions to PNUE were not significant (Figure S1). Indeed, A_{mass} and N_m were positively correlated across species (LES SMA $r^2 = 0.34$). Therefore, coordinating g_m, C_i and P_R to maximize A_{mass} per unit of leaf nitrogen is the prior biological strategy adopted by plants to obtain high PNUE in the process of evolution (Figure 6d). According to earlier research, C_i varied slightly among species grown under non-stress conditions in the current atmospheric CO_2 conditions (von Caemmerer and Farquhar, 1981; Evans *et al*., 2009). In the global database, the coefficient of variation (CV) for C_i was 0.15, which was much lower than the CV of C_c (0.31). It might be reasonable to infer that g_m, rather than g_{sw}, plays a critical role in determining C_c across non-stressed plant species (Ethier and Livingston, 2004; Tosens *et al*., 2012; Onoda *et al*., 2017). Bryophytes have thick cell walls and no stomatal conductance structure. Therefore, it's better to choose common leaf traits as bio-indicators to explore PNUE global variations of terrestrial plants. Cell walls (CWs) have been recognized for their importance in plant physiology and biotechnology, and recent reviews have suggested that T_{cwm} could be crucial in regulating photosynthesis (Flexas and Carriquí, 2020; Flexas *et al*., 2021). In the following sections, T_{cwm}-mediated physiological mechanisms controlling PNUE variations through land plant phylogeny have been discussed.

The P_R and g_m have been considered two important factors underlying PNUE variations in seed plants (Hikosaka, 2004; Onoda *et al*., 2017). Our results demonstrated that 65% of PNUE variations in the global dataset are explained by the two variables. There are synergetic effects of the two traits on PNUE across plant phylogeny, which means an increase in either of them could contribute to the improvement of PNUE. However, the synergetic effect of P_R is determined by g_m. A slight improvement in PNUE is observed in species with low g_m owing to an increase in P_R; whereas a double increment in PNUE is observed in species with high g_m (Fig. 4a). CO_2 enrichments inside chloroplasts owning to high g_m facilitate photosynthesis and subsequently a significant increment in PNUE is anticipated. Warren and Adams (2006) suggested that variation in the g_m–photosynthesis relationship contributes to variation in PNUE. Their suggestion is supported and underlying mechanisms are addressed by our results that photosynthesis is strongly restricted by g_m in species with low $g_m < 0.001$ mol g^{-1} s^{-1} (Figure 4b); in contrast, the biochemical limitation is a major factor constraining photosynthesis in high-g_m species. Greater improvement in PNUE is achieved in high-g_m species than the low-g_m species in condition of the same P_R. The g_m threshold where the relative importance of P_R and g_m in determining PNUE shifts might be 0.001 mol g^{-1} s^{-1}, corresponding to the area-based g_m from 0.05 to 0.1 mol m^{-2} s^{-1}. Xiong and Flexas (2018) evaluated the covariance in A_{mass}, g_m, and Rubisco concentrations in hundreds of rice varieties, finding low g_m limitation and strong biochemical limitation in modern varieties. PNUE improvement in modern varieties would be facilitated by the improvement of carboxylation capacity. A pronounced increment in PNUE would be possible in high-g_m species via efforts to ameliorate carboxylation efficiency. Collectively, PNUE variations across major plant groups are strongly regulated by P_R and g_m, with their interactive effects varying depending on g_m.

The g_m is a composite conductance of the CO_2 diffusion pathway between the substomatal cavities and carboxylation sites within chloroplasts. Earlier studies emphasized the importance of cell wall composition (Ellsworth *et al*., 2018; Carriquí *et al*., 2020; Roig-Oliver *et al*., 2021), cell wall porosity (Evans *et al*., 2009), cell wall thickness (Carriquí *et al*., 2015, 2019, 2021; Flexas *et al*., 2021), and chloroplast distribution, in particular the S_c (Carriquí *et al*., 2015, 2019; Tosens *et al*., 2016; Han *et al*., 2018; Du *et al*., 2019; Ren *et al*., 2019; Nadal *et al*., 2021), in determining g_m. Our findings indciated a strong and positive correlation between g_m and S_c, while a

significantly negative relationship between g_m and T_{cwm} across major plant groups and through phylogeny (Figures 5c and d; Figure 6a). There is an exponential decline tendency in g_m with increasing T_{cwm}, and the low g_m value tends to level off at greater T_{cwm} (Figure S5), implying that species with thicker cell walls might have the same g_m in comparison to those with relatively thin cell walls. According to Nadal *et al*. (2021), substantial S_c could compensate for thick cell wall limitation to achieve relatively high g_m in resurrection plants with thick T_{cwm}. A large range of g_m at given T_{cwm} in Figure 5c mainly arises from differences in S_c among species. The negative correlation between S_c and T_{cwm} across major plant groups suggests high S_c clustering at the low-end of T_{cwm} axis. Optimal arrangement of chloroplast position along cell walls could minimize CO_2 diffusion resistance at liquid phase and enlarge surface area of bicarbonate ion diffusion, contributing to g_m.

In the context of vegetation model parameterization, P_R global patterns were deduced from the known LMA global map using a P_R–LMA relationship (Luo *et al*., 2021). In line with their reports, the P_R is inversely scaled with LMA (Figure 5a), and the relationship is analogous to the g_m–T_{cwm} relationship. There is a progressive phylogenetic trend associated with LMA and T_{cwm} in spermatophyta: from low LMA and thin T_{cwm} in angiosperms to high LMA and large T_{cwm} in gymnosperms (Onoda *et al*., 2017; Flexas *et al*., 2021; Xing *et al*., 2021), while an exception occurred in mosses and ferns that have low LMA (Tosens *et al*., 2016; Carriquí *et al*., 2019). Interestingly, there is a consistent phylogenetic trend regarding T_{cwm} from bryophytes to angiosperms reported in the study of Gago *et al*. (2019) and in Figure 6b: from very large T_{cwm} in bryophytes to very low T_{cwm} in angiosperms. Indeed, higher correlation strength is attained when scaling g_m with T_{cwm} in comparison to g_m–LMA (Figures 5b and c and Figure 6a). When g_m changes with T_{cwm}, the log-transformed g_m–T_{cwm} correlation exhibits more convergent characteristics (i.e., g_m converges at given T_{cwm}). It indicated that the P_R–T_{cwm} correlation is likely synonymous with the exponential decay correlation of P_R–LMA, or at least ought to be. Theoretical predictions by Evans *et al.* (2009) revealed that other elements in the mesophyll CO_2 diffusion pathway of the liquid phase could co-vary with T_{cwm}, such as the decrease in Rubisco per unit of exposed chloroplast surface area and thinner chloroplast with increasing T_{cwm}. If the P_R, which is proportional to photosynthesis, did not decrease with increases in T_{cwm}, then the internal CO_2 drawdown would have been substantially higher than observations. Assuming independence of P_R on T_{cwm}, the ten-fold decline

of g_m owning to an increase in T_{cwm} from 0.2 to 0.5 μm (e.g., the g_m decline from 0.004 to 0.0004 mol g^{-1} s^{-1}) would amplify the internal CO_2 drawdown by more than five folds in species featured by T_{cwm} of 0.5 μm, and a strong correlation between DeltaC and T_{cwm} would therefore be observed. However, this expectation contradicts the fact that the actual increase of the CO_2 drawdown is limited to 50% over a wide range of T_{cwm} (Figure 5f). The decrease in P_R with T_{cwm} ultimately balances the increase in mesophyll resistance, resulting in the CO_2 drawdown that is only weakly proportional to T_{cwm} (Figure 5f). The experimental results in this study, i.e., a significantly negative correlation between T_{cwm} and $P_{R,}$ corroborate the theoretical prediction of the T_{cwm}–biochemical capacity offset mechanisms in the study of Evans *et al*. (2009) (Figure 5e and Figure 6a). In our study, the observed significance of the P_R–T_{cwm} relationship across major plant groups is consistent with the findings in the study by Onoda *et al*. (2017) for seed plants. However, the anticipated inverse correlation between chloroplast thickness and T_{cwm} is not observed (Figure S6). The thickness of photosynthetic tissues is one of the distinctive differences in leaf anatomy among bryophytes, ferns, and spermatophytes (Han *et al*., 2018; Carriquí *et al*., 2019). The chloroplast amount per leaf mass may co-vary with T_{cwm} from bryophytes to angiosperms, resulting in the observed P_R–T_{cwm} relationship. It was unclear and open to interpretation whether the response pattern of P_R to T_{cwm} was exclusively independent or dependent causality owing to g_m changes. The possibility of g_m effects on the observed P_R–T_{cwm} response pattern could be excluded as no strong correlations are observed for the P_R–g_m relationship (Figure 3d) and the V_{cmax}–C_c relationship (Figure S7). It was proposed that T_{cwm} is the critical factor controlling evolutionary modifications of PNUE from bryophytes to angiosperms based on the generality of significant correlations for P_R–T_{cwm} and g_m–T_{cwm} in the worldwide database.

Mosses and ferns are widely distributed across the globe, being dominant species in various habitats ranging from understory to full sunlight environment and from hot and moist lands to cold and dry lands. A recent study demonstrated that the paired-trait correlations in leaf economics spectrum in ferns are independent of growth light and nutrient gradients (Li *et al*., 2022). Results in 75 woody species in subtropical forests in the study by Chen *et al*. (2020) revealed a unified trade-off relationship in paired traits under different light gradients. Differences in between-species responses to changes in light conditions in trees and shrubs arise from significant shifts in the intercept of the SMA regression line not the scaling slope (Keenan and Niinemets,

2016), which might be explained by either leaf habits or the height-based economics spectrum (Zhao *et al*., 2017). Species-level acclimations to habitat irradiance could not be strong enough to change the relative positions of moss species along trait axes (Waite and Sack, 2009; Z. Wang *et al*., 2017). Most deviations of bryophytes in A_{mass}–LMA and PNUE–LMA relationships in comparison to angiosperms are attributed to fundamental difference between the two plant groups. Our results concerning underpinnings of PNUE variations from bryophytes to angiosperms are reliable.

Materials and Methods

Data collection

In this study, we constructed a global collection of leaf morphological, anatomical, and physiological traits of non-stressed mature leaves of terrestrial C_3 species comprising major plant groups and phylogeny. The dataset included the photosynthetic organs with various morphologies (e.g. phyllidia or thalli in mosses and lichen species). LMA and leaf thickness (T_{leaf}), chloroplast surface area exposed to intercellular airspace per unit leaf area (S_c), mesophyll surface area exposed to intercellular airspace per unit leaf area (S_m), cytoplasm thickness (T_{cyt}), mesophyll cell wall thickness (T_{cwm}), mesophyll thickness (T_{mes}), chloroplast thickness (T_{chl}), the fraction of intercellular air space (f_{ias}), the average distance between the chloroplast and the cell wall (cytoplasm thickness, L_{ct}) were among the structural and anatomical traits of the leaf. Physiological traits comprised photosynthetic capacity at normal atmospheric CO_2 concentration and saturation light (A_{mass}, mass-based photosynthesis rate), leaf nitrogen content per leaf mass (N_{mass}), stomatal conductance to water vapor (g_{sw}), intercellular and chloroplastic CO_2 concentration (C_i and C_c, respectively), g_m, the C_c-based maximum carboxylation rate (V_{cmax}), the maximum electron transport rate (J_{max}), stomatal limitation on photosynthesis (l_s), mesophyll limitation on photosynthesis (l_m), biochemical limitation on photosynthesis (l_b), and leaf temperature (L_{temp}). In this study, articles that highlighted keywords, such as “mesophyll conductance” or “internal conductance” archived by the Web of Science (https://www.webofscience.com) and the China National Knowledge Infrastructure (https://www.cnki.net) until July 2022 were considered. Trait measurements in most species including ferns and moss species in the field and/or outdoor conditions under the most favorable growing conditions (i.e., with the least amount of environmental

stress), were considered reliable for use. Measurements of shade-adapted leaves within plant canopies were not included in the global dataset.

The data collection campaign was challenging as the number of available traits varied among surveyed articles. If the traits could be inferred by supporting information in articles, the inferred values were restored to the global database. Indeed, it is impossible to determine the CO_2 concentration within the chloroplast stroma. The internal CO_2 drawdown (DeltaC, the difference between C_i and C_c) was inferred according to Fick's first law: DeltaC = $C_a - A(1.56/g_{sw} - 1/g_m)$, which was commonly adopted in leaf photosynthesis-stomatal conductance coupled model (Onoda *et al*., 2017; Xue *et al*., 2022). It was discovered that bryophytes are the only group of plants that are completely devoid of stomata. Hence, the DeltaC values in bryophytes species were inferred using the equation of, DeltaC = A/g_m. The global C_a of 380 ppm was applied in the absence of C_a data in surveyed articles.

The P_R was calculated using two different methods: a numerical calculation method using V_{cmax} and N_{area} as demonstrated by Niinemets and Tenhunen (1997), and a chemical assay of Rubisco content. The Sharkey online calculator (Sharkey *et al*., 2007) and optimization inversion algorithms were two common methods to estimate V_{cmax} from the A/C_i curve (Xue *et al*., 2022). The estimated V_{cmax} values by the parameter estimation methods were comparable among plant species, since Rubisco kinetics parameters in 89% of surveyed articles were consistently taken from the study of Bernacchi *et al*. (2002). Variation in Rubisco kinetics parameters measured *in vitro* was less than 10% among C_3 plant species (von Caemmerer, 2020), which was far less than the 10-fold variations of inter-specific A_{mass} at a given LMA (Figure 1d). Hence, their Rubisco kinetics parameters might be highly recommended for V_{cmax} calculations across major plant functional types, as commonly did in surveyed articles. The P_R dataset derived from the chemical assay in the study of Onoda *et al*. (2017) was solely limited to spermatophyte. By combing P_R numerical calculations, the P_R dataset was expanded to enrich species diversity in the global dataset. In the global dataset, all leaf traits were measured in sunlit leaves around 25^oC with relatively high incident radiation and ambient atmospheric CO_2 concentration. The P_R assessments by the numerical method were sensitive to measuring temperatures (Niinemets and Tenhunen, 1997). According to Medlyn *et al*. (2002), temperature response functions of V_{cmax} and J_{max} with activation energy (ΔH_a)

at 63.0 kJ mol^{-1} were used to convert the values of V_{cmax} and J_{max} measured at other leaf temperatures to values at standard temperature.

Except for the DeltaC and P_R, other values of physiological and morpho-anatomical traits were directly retrieved from the surveyed articles. To prevent the impact of environmental stress on analysis, leaf trait data from the same species reported by various studies were averaged for use when environmental conditions sensed by the species were optimal (Poorter *et al*., 2009; Poorter *et al*., 2011; Xing *et al*., 2021). Wild, old and modern crop kinds differed significantly in leaf morpho-physiological traits, being representatives of angiosperm species in leaf economics spectrum evolving towards high photosynthetic efficiency (Xiong and Flexas, 2018; Martin *et al*., 2018; Hayes *et al*., 2019). In such case, physiological and morpho-anatomical traits in crops and non-crop plants were merged for data analysis. Collectively, there were 1296 lines of data in 679 species, covering major life forms in land plants, such as bryophytes (57 lines in mosses and lichen species), pteridophytes (64 lines in ferns and fern allies species), gymnosperm (83 lines in needles and scales leaved species), and angiosperm (1092 lines in trees, shrubs, grass and crops).

Data analysis

Data of all traits were log_{10}-transformed before correlation analysis, which was a common practice adopted in ecological studies because data types of some leaf traits do not follow a normal distribution (Wright *et al*., 2005; Carriquí *et al*., 2015; Tosens *et al*., 2016; Onoda *et al*., 2017; Carriquí *et al*., 2019). The strength of bivariate trait correlation was assessed using the standardized major axis slope (SMA, also known as reduced major axis slopes), a method frequently practiced in these studies, was applied to determine. The non-parametric regression model (locally weighted regression, Loess) used by Xue *et al*. (2021) and Kurmangozhinov *et al*. (2020) to clarify threshold at which trait strong coupling shifted to weak coupling was used for paired traits with significant curvilinear relationship, rise to the maximum or decline to the minimum curve trajectory. Indeed, it is the mass-based physiological traits, such as A_{mass} that determine the biochemical capacity of single cells and are the important factors in the global trade-off between the physiological and structural traits of foliage (Niinemets and Tenhunen, 1997; Wright *et al*., 2005; Tosens *et al*., 2016; Onoda *et al*., 2017). We found that the area-based trait analysis exhibited analogous

results in correlation analysis as the expression of the mass-based traits. Thus, the mass-based physiological traits were employed for correlation analysis unless otherwise indicated. Prior to paired trait correlation analysis, a phylogenetic tree was constructed for all species using the megatree approach in the R package V.PhyloMaker and phylogenetic signals were estimated using Pagel's λ following Xing *et al.* (2021). There were 39 species failing to be bound to the constructed phylogenetic tree as they were not present in the plantlist database of the V.PhyloMaker package (package acquiring date: 2022/05/13). Of the 39 species, *Polistichium aculeatum* (pteridophyte) was one, and the remaining belonged to the bryophytes.

In R 4.0.5 software (R Core Team, 2021), the paired-trait correlation analysis using the smart-package, Loess model application, and phylogenetic signal analysis using the V.PhyloMaker package were performed. Structural equation modeling (SEM) was applied to explore how morpho-physiological traits influence PNUE variations (Shipley, 2004). The estimator to parameterize the SEM was the maximum likelihood method. Using the comparative fit index (CFI, > 0.9), p-value, and the standard root mean squared residual (SRMR, < 0.08) (Shipley, 2004), appropriate SEM model fit was inspected. The semPlot package in the R software was used to visualize the SEM analysis that was performed using the lavaan package (Rosseel, 2012).

The relative importance of P_R and g_m in relation to PNUE variations was quantified using the photosynthetic coordination theory. According to the biochemical photosynthesis model established by Farquhar *et al*. (1980), the photosynthetic rate is constrained by either the Rubisco carboxylation rate at low Rubisco content and CO_2 concentrations (A_c) or the RuBP regeneration rate at comparatively high CO_2 concentrations owning to low electron transport rates (A_j). The A_c value is primarily determined by V_{cmax}, followed by C_c at a given leaf temperature, (Eqn. 1). Besides the direct effects of P_R on photosynthesis, the effects of g_m on photosynthesis are realized through their impacts on C_c (Ethier and Livingston, 2004; Evans *et al*., 2009; Kaldenhoff, 2012; Tosens *et al*., 2012; Onoda *et al*., 2017; Gómez-Ocampo *et al*., 2021). The photosynthetic coordination theory was originally proposed by von Caemmerer and Farquhar (1981) and further modified by Maire *et al.* (2012) in 31 individual C_3 species. H. Wang *et al*. (2017), Smith *et al*. (2019), and Harrison *et al.* (2021) in regional vegetation studies stated that photosynthesis tends to be co-limited

by electron transport and carboxylation under typical environmental conditions, thus maximizing potential resource use for growth and reproduction. The P_R and g_m functioning effects on inter-specific PNUE variations could be predicted quantitatively using the photosynthetic coordination theory. The PNUE could be expressed with Eqn. 3 that was derived from Eqn. 1 and 2 as follows:

$$A_{area} = \left(1 - \frac{\Gamma^*}{C_c}\right) A_c - R_d = \left(1 - \frac{\Gamma^*}{C_c}\right) \frac{V_{cmax} C_c}{C_c + K_m} - R_d \quad (1)$$

$$\frac{A_{area}}{N_{area}} = \left(1 - \frac{\Gamma^*}{C_c}\right) \frac{V_{cmax}/N_{area}}{1 + K_m/C_c} - \frac{R_d}{N_{area}} \quad (2)$$

$$PNUE = \left(1 - \frac{\Gamma^*}{C_c}\right) \frac{6.25 V_{cr}}{1 + K_m/C_c} P_R - \frac{R_d}{N_{area}} \quad (3)$$

where V_{cr} is the maximum carboxylation rate per unit Rubisco protein (47.34 μmol CO_2 (g Rubisco)$^{-1}$ s^{-1} at 25°C) and 6.25 is the nitrogen content of Rubisco protein (Niinemets and Tenhunen, 1997; Luo *et al*., 2021); R_d is area-based dark respiration in the light; Γ* is the chloroplast CO_2 compensation point, corresponding to 42.75 μmol mol^{-1} at 25°C. K_m is equal to $K_c(1+O/K_o)$, where K_c and K_o are the Michaelis–Menten constants for CO_2 and O_2, respectively (Bernacchi *et al*., 2002). The PNUE simulations were generated considering a continuous series of P_R and C_c. We hypothesized that the effect of g_m on PNUE were more obvious across contrasting plant groups with significant differences in g_m in comparison to several randomly selected species. As a result, the species in the global dataset were divided into two groups according to their g_m values, such as the high- and low-g_m species assembles. The high-g_m species assemble exhibited g_m from 0.25 to 0.32 mol m^{-2} s^{-1}, and the low-g_m species assemble had g_m from 0.05 to 0.06 mol m^{-2} s^{-1}, corresponding to C_c at approximately 100 and 230 μmol mol^{-1} in leaves under current atmospheric CO_2 conditions, respectively. The PNUE theoretical analysis was cross-validated using the PNUE and P_R measurements together with g_m and C_c measurements (i.e., trait values taken/inferred from the surveyed articles) in the two species assembles. Variations in predicted PNUE were assumed to be independent of the intercept R_d/N_{area}.

Acknowledgments

This work was supported by the National Natural Science Foundation of China (32001129) and Estonian Research Council (PUT 1473).

Author contributions:

Conceptualization and investigation: DDL, WX

Methodology, supervision, visualization and Writing-original draft: WX

Writing-review & editing: MC, DLX, TT, YCX, WX

Competing interests: Authors declare that they have no competing interests.

Data and materials availability: All data are available in the supplementary materials.

References

Anderegg L.D.L., Berner L.T., Badgley G., Sethi M.L., Law B.E., HilleRisLambers J. (2018). Within-species patterns challenge our understanding of the leaf economics spectrum. Ecology Letters, **21**: 734-744.

Bahar N.H.A., Hayes L., Scafaro A.P., Atkin O.K., Evans J.R. (2018). Mesophyll conductance does not contribute to greater photosynthetic rate per unit nitrogen in temperate compared with tropical evergreen wet-forest tree leaves. New Phytologist, **218**: 492-505.

Bernacchi C.J., Portis A.R., Nakano H., von Caemmerer S., Long S.P. (2002). Temperature response of mesophyll conductance. Implications for the determination of Rubisco enzyme kinetics and for limitations to photosynthesis in vivo. Plant Physiology, **130**: 1992-1998.

Carriquí M., Cabrera H.M., Conesa M.À., Coopman R.E., Douthe C., Gago J., Gallé A., Galmés J., Ribas-Carbo M., Tomás M. et al. (2015). Diffusional limitations explain the lower photosynthetic capacity of ferns as compared with angiosperms in a common garden study. Plant, Cell & Environment, **38**: 448-460.

Carriquí M., Roig-Oliver M., Brodribb T.J., Coopman R., Gill W., Mark K., Niinemets Ü., Perera-Castro A.V., Ribas-Carbó M., Sack L. et al. (2019). Anatomical constraints to nonstomatal diffusion conductance and photosynthesis in lycophytes and bryophytes. New Phytologist, **222**: 1256-1270.

Carriquí M., Nadal M., Clemente-Moreno M.J., Gago J., Miedes E., Flexas J. (2020). Cell wall composition strongly influences mesophyll conductance in gymnosperms. The Plant Journal, **103**: 1372-1385.

Carriquí M., Nadal M., Flexas J. (2021). Acclimation of mesophyll conductance and anatomy to light during leaf aging in *Arabidopsis thaliana*. Physiologia Plantarum, **172**: 1894-1907.

Chen X., Sun J., Wang M., Lyu M., Niklas K.J., Michaletz S.T. Zhang Q., Chen D. (2020). The leaf economics spectrum constrains phenotypic plasticity across a light gradient. Frontiers in Plant Science, **11**: 735.

De Bello F., Carmona C., Dias A., Götzenberger L., Moretti M., Berg M. (2021). Handbook of Trait-Based Ecology: From Theory to R Tools. Cambridge: Cambridge University Press.

Du Q.J., Liu T., Jiao X., Song X.M., Zhang J.Y., Li J.M. (2019). Leaf anatomical adaptations have central roles in photosynthetic acclimation to humidity. Journal of Experimental Botany, **70**: 4949-4961.

Ellsworth P.V., Ellsworth P.Z., Koteyeva N.K., Cousins A.B. (2018). Cell wall properties in *Oryza sativa* influence mesophyll CO_2 conductance. New Phytologist, **219**: 66-76.

Ethier G.J., Livingston N.J. (2004). On the need to incorporate sensitivity to CO_2 transfer conductance into the Farquhar–von Caemmerer–Berry leaf photosynthesis model. Plant, Cell & Environment, **27**: 137-153.

Evans J.R., Kaldenhoff R., Genty B., Terashima I. (2009). Resistances along the CO_2 diffusion pathway inside leaves. Journal of Experimental Botany, **60**: 2235-2248.

Evans J.R. (2021). Mesophyll conductance: walls, membranes and spatial complexity. New Phytologist, **229**: 1864-1876.

Farquhar G.D., von Caemmerer S., Ball J.A. (1980). A biochemical model of photosynthetic CO_2 assimilation in leaves of C_3 species. Planta, **149**: 78-90.

Flexas J., Carriquí M. (2020). Photosynthesis and photosynthetic efficiencies along the terrestrial plant's phylogeny: lessons for improving crop photosynthesis. The Plant Journal, **101**: 964-978.

Flexas J., Clemente-Moreno M.J., Bota J., Brodribb T.J., Gago J., Mizokami Y., Nadal M., Perera-Castro A.V., Roig-Oliver M., Sugiura D. et al. (2021). Cell wall thickness and composition are involved in photosynthetic limitation. Journal of Experimental Botany, **72**: 3971-3986.

Gago J., Carriquí M., Nadal M., Clemente-Moreno M.J., Coopman R.E., Fernie A.R., Flexas J. (2019). Photosynthesis optimized across land plant phylogeny. Trends in Plant Science, **24**: 947-958.

Garnier E., Gobin O., Poorter H. (1995). Nitrogen productivity depends on photosynthetic nitrogen use efficiency and on nitrogen allocation within the plant. Annals of Botany, **76**: 667-672.

Gómez-Ocampo G., Ploschuk E.L., Mantese A., Crocco C.D., Botto J.F. (2021). BBX21 reduces abscisic acid sensitivity, mesophyll conductance and chloroplast electron transport capacity to increase photosynthesis and water use efficiency in potato plants cultivated under moderated drought. The Plant Journal, **108**: 1131-1144.

Gvozdevaite A., Oliveras I., Domingues T.F., Peprah T., Boakye M., Afriyie L., da Peixoto S.K., de Farias J., de Oliveira A.E., Farias A. et al. (2018). Leaf-level photosynthetic capacity dynamics in relation to soil and foliar nutrients along forest–savanna boundaries in Ghana and Brazil. Tree Physiology, **38**: 1912-1925.

Han J.M., Lei Z.Y., Flexas J., Zhang Y.J., Carriqui M., Zhang W.F., Zhang Y.L. (2018). Mesophyll conductance in cotton bracts: anatomically determined internal CO_2 diffusion constraints on photosynthesis. Journal of Experimental Botany, **69**: 5433-5443.

Harrison S.P., Cramer W., Franklin O., Prentice I.C., Wang H., Brännström Å., de Boer H., Dieckmann U., Joshi J., Keenan T.F., Lavergne A. (2021). Eco-evolutionary optimality as a means to improve vegetation and land-surface models. New Phytologist, **231**: 2125-2141.

Hayes F.J., Buchanan S.W., Coleman B., Gordon A.M., Reich P.B., Thevathasan N.V., Wright I.J., Martin A.R. (2019). Intraspecific variation in soy across the leaf economics spectrum. Annals of Botany, **123**: 107-120.

Hidaka A., Kitayama K. (2009). Divergent patterns of photosynthetic phosphorus-use efficiency versus nitrogen-use efficiency of tree leaves along nutrient-availability gradients. Journal of Ecology, **97**: 984-991.

Hikosaka K., Hanba Y.T., Hirose T., Terashima I. (1998). Photosynthetic nitrogen-use efficiency in leaves of woody and herbaceous species. Functional Ecology, **12**: 896-905.

Hikosaka K. (2004). Interspecific difference in the photosynthesis-nitrogen relationship: patterns, physiological causes, and ecological importance. Journal of Plant Research, **117**: 481-494.

Hikosaka K. (2010). Mechanisms underlying interspecific variation in photosynthetic capacity across wild plant species. Plant Biotechnology, **27**: 223-229.

Kaldenhoff R. (2012). Mechanisms underlying CO_2 diffusion in leaves. Current Opinion in Plant Biology, **15**: 276-281.

Keenan T.F., Niinemets Ü. (2016). Global leaf trait estimates biased due to plasticity in the shade. Nature Plants, **3**: 16201.

Kurmangozhinov A., Xue W., Li X., Zeng F., Sabit R., Tusun T. (2020). High biomass production with abundant leaf litterfall is critical to ameliorating soil quality and productivity in reclaimed sandy desertification land. Journal of Environmental Management, **263**: 110373.

Lei Z.Y., Wang H., Wright I.J., Zhu X.G, Niinemets Ü., Li Z.L., Sun D.S., Dong N., Zhang W.F., Zhou Z.L. et al. (2021a). Enhanced photosynthetic nitrogen use efficiency and increased nitrogen allocation to photosynthetic machinery under cotton domestication. Photosynthesis Research, **150**: 239-250.

Lei .Z, Liu F., Wright I.J., Carriquí M., Niinemets Ü., Han J., Jia M., Atwell B.J., Cai X., Zhang W. et al. (2021b). Comparisons of photosynthetic and anatomical traits between wild and domesticated cotton. Journal of Experimental Botany, **73**: 873-885.

Li J., Chen X.P., Wu P.P., Niklas K.J., Lu Y.M., Zhong Q.L., Hu D.D., Cheng L., Cheng D.L. (2022). The fern economics spectrum is unaffected by the environment. Plant, Cell & Environment **45**: 3205-3218.

Luo X., Keenan T.F., Chen J.M., Croft H., Prentice C.I., Smith N.G., Walker A.P., Wang H., Wang R., Xu C. et al. (2021). Global variation in the fraction of leaf nitrogen allocated to photosynthesis. Nature Communications, **12**: 4866.

Maire V., Martre P., Kattge J., Gastal F., Esser G., Fontaine S., Soussana J.F. (2012). The coordination of leaf photosynthesis links C and N fluxes in C_3 plant species. PloS One, **7**: e38345.

Martin A.R., Hale C.E., Cerabolini B.E.L., Cornelissen J.H.C., Craine J., Gough W.A., Kattge J., Tirona C.K.F. (2018). Inter- and intraspecific variation in leaf economic traits in wheat and maize. AoB Plants, **10**: ply006.

Medlyn B.E., Dreyer E., Ellsworth D., Forstreuter M., Harley P.C., Kirschbaum M.U.F., Le Roux X., Montpied P., Strassemeyer J., Walcroft A. (2002). Temperature response of parameters of a biochemically based model of photosynthesis. II. A review of experimental data. Plant, Cell & Environment, **25**: 1167-1179.

Nadal M., Perera-Castro A.V., Gulías J., Farrant J.M., Flexas J. (2021). Resurrection plants optimize photosynthesis despite very thick cell walls by means of chloroplast distribution. Journal of Experimental Botany, **72**: 2600-2610.

Niinemets Ü., Tenhunen J.D. (1997). A model separating leaf structural and physiological effects on carbon gain along light gradients for the shade-tolerant species *Acer saccharum*. Plant, Cell & Environment, **20**: 845-866.

Oguchi R., Ozaki H., Hanada K., Hikosaka K. (2016). Which plant trait explains the variations in relative growth rate and its response to elevated carbon dioxide concentration among Arabidopsis thaliana ecotypes derived from a variety of habitats? Oecologia, **180**: 865-876.

Onoda Y., Hikosaka K., Hirose T. (2004). Allocation of nitrogen to cell walls decreases photosynthetic nitrogen-use efficiency. Functional Ecology, **18**: 419-425.

Onoda Y., Wright I.J., Evans J.R., Hikosaka K., Kitajima K., Niinemets Ü., Poorter H., Tosens T., Westoby M. (2017). Physiological and structural tradeoffs underlying the leaf economics spectrum. New Phytologist, **214**: 1447-1463.

Popper, Z.A., Fry S. (2003). Primary cell wall composition of bryophytes and charophytes. Annals of Botany, **91**: 1-12.

Preston C.D., Hill M.O. (1999). The geographical relationships of the British and Irish flora: a comparison of pteridophytes, flowering plants, liverworts and mosses. Journal of Biogeography, **26**: 629-642.

Pons T.L., Westbeek M.H.M. (2004). Analysis of differences in photosynthetic nitrogen-use efficiency between four contrasting species. Physiologia Plantarum, **122**: 68-78.

Poorter H., Evans J.R. (1998). Photosynthetic nitrogen-use efficiency of species that differ inherently in specific leaf area. Oecologia, **116**: 26-37.

Poorter H., Niinemets Ü., Poorter L., Wright I.J., Villar R. (2009). Causes and consequences of variation in leaf mass per area (LMA): a meta-analysis. New Phytologist, **182**: 565-588.

Poorter H., Remkes C., Lambers H. (1990). Carbon and nitrogen economy of 24 wild species differing in relative growth rate. Plant Physiology, **94**: 621-627.

Popper Z.A., Michel G., Herve C., Domozych D.S., Willats W.G.T., Tuohy M.G., Kloareg B., Stengel D.B. (2011). Evolution and diversity of plant cell walls: From algae to flowering plants. In: Merchant, S.S., Briggs, W.R., Ort, D. (Eds.), Annual Review of Plant Biology, **62**, pp.567.

R Core Team. (2021). R: A Language and Environment for Statistical Computing; R Foundation for Statistical Computing: Vienna, Austria, Available online: https://www.R-project.org/ (accessed on May 2022).

Reich P.B., Ellsworth D.S., Walters M.B. (1998). Leaf structure (specific leaf area) modulates photosynthesis-nitrogen relations: evidence from within and across species and functional groups. Functional Ecology, **12**: 948-958.

Ren T., Weraduwage S.M., Sharkey T.D. (2019). Prospects for enhancing leaf photosynthetic capacity by manipulating mesophyll cell morphology. Journal of Experimental Botany, **70**: 1153-1165.

Ripullone F., Grassi G., Lauteri M., Borghetti M. (2003). Photosynthesis–nitrogen relationships: interpretation of different patterns between *Pseudotsuga menziesii* and *Populus* × *euroamericana* in a mini-stand experiment. Tree Physiology, **23**: 137-144.

Roig-Oliver M., Douthe C., Bota J., Flexas J. (2021). Cell wall thickness and composition are related to photosynthesis in Antarctic mosses. Physiologia Plantarum, **173**: 1914-1925.

Rosseel Y. (2012). Lavaan: an R package for structural equation modeling. Journal of Statistical Software, **48**: 1-36.

Sharkey T.D., Bernacchi C.J., Farquhar G.D., Singsaas E.L. (2007). Fittingphotosynthetic carbon dioxide response curves for C_3 leaves. Plant, Cell & Environment, **30**: 1035-1040.

Shipley B., Lechowicz M.J., Wright I., Reich P.B. (2006). Fundamental trade-offs generating the worldwide leaf economics spectrum. Ecology, **87**: 535-541.

Shipley B. (2004). Cause and correlation in biology: A user's guide to path analysis, structural equations and causal inference. Cambridge University Press, Cambridge, UK.

Smith N.G., Keenan T.F., Prentice C.I., Wang H., Wright I.J., Niinemets Ü., Crous K.Y., Domingues T.F., Guerrieri R., Ishida Y., et al. (2019). Global photosynthetic capacity is optimized to the environment. Ecology Letters, **22**: 506-517.

Takashima T., Hikosaka K., Hirose T. (2004). Photosynthesis or persistence: nitrogen allocation in leaves of evergreen and deciduous *Quercus species*. Plant, Cell & Environment, **27**: 1047-1054.

Tosens T., Niinemets Ü., Vislap V., Eichelmann H., Castro-Díez P. (2012). Developmental changes in mesophyll diffusion conductance and photosynthetic capacity under different light and water availabilities in *Populus tremula*: how structure constrains function. Plant, Cell & Environment, **35**: 839-856.

Tosens T., Nishida K., Gago J., Coopman R.E., Cabrera H.M., Carriquí M., Laanisto L., Morales L., Nadal M., Rojas R., et al. (2016). The photosynthetic capacity in 35 ferns and fern allies: mesophyll CO_2 diffusion as a key trait. New Phytologist, **209**: 1576-1590.

von Caemmerer S., Farquhar G.D. (1981)**.** Some relationships between the biochemistry of photosynthesis and the gas exchange of leaves. Planta, **153**: 376-387.

von Caemmerer S. (2020). Rubisco carboxylase/oxygenase: from the enzyme to the globe: a gas exchange perspective. Journal of Plant Physiology, **252**, 153240.

Waite M, Sack L. (2009). How does moss photosynthesis relate to leaf and canopy structure? Trait relationships for 10 Hawaiian species of contrasting light habitats. New Phytologist, **185**: 156-172.

Wang M., Yuan D., Gao W., Li Y., Tan J., Zhang X. (2013). A comparative genome analysis of PME and PMEI families reveals the evolution of pectin metabolism in plant cell walls. Plos One, **8**: e72082.

Wang Z., Liu X., Bader M., Feng D., Bao W. (2017). The "plant economic spectrum" in bryophytes, a comparative study in subalpine forest. American Journal of Botany, **104**: 261-270.

Wang H., Prentice I.C., Keenan T.F., Davis T.W., Wright I.J., Cornwell W.K., Evans B.J., Peng C. (2017). Towards a universal model for carbon dioxide uptake by plants. Nature Plants, **3**: 734-741.

Warren C.R., Adams M.A. (2006). Internal conductance does not scale with photosynthetic capacity: implications for carbon isotope discrimination and the economics of water and nitrogen use in photosynthesis. Plant, Cell & Environment, **29**: 192-201.

Warren C.R., Adams M.A. (2000). Trade-offs between the persistence of foliage and productivity in two Pinus species. Oecologia, 124: 487-494.

Wright I.J., Reich P.B., Cornelissen J.H.C., Falster D.S., Garnier E., Hikosaka K., Lamont B.B., Lee W., Oleksyn J., Osada N. (2005). Assessing the generality of global leaf trait relationships. New Phytologist, **166**: 485-496.

Xing K., Niinemets Ü., Rengel Z., Onoda Y., Xia J., Chen H.Y.H., Zhao M., Han W., Li H. (2021). Global patterns of leaf construction traits and their covariation along climate and soil environmental gradients. New Phytologist, **232**: 1648-1660.

Xiong D., Flexas J. (2018). Leaf economics spectrum in rice: leaf anatomical, biochemical, and physiological trait trade-offs. Journal of Experimental Botany, **69**: 5599-5609.

Xue W., Li X., Zeng F. (2021). Inter-annual variations of seed cotton yield in relation to soil organic carbon and harvest index in reclaimed desertified land. Field Crops Research, **272**: 108267.

Xue W., Luo H., Carriquí M., Nadal M., Huang J.F., Zhang J.L. (2022). Quantitative expression of mesophyll conductance temperature response in the FvCB model and impacts on plant gas exchange estimations. Agricultural and Forest Meteorology, **325**: 109153.

Yin L.J., Xu H.C., Dong S.X., Chu J.P., Dai X.L., He M.R. (2019). Optimised nitrogen allocation favors improvement in canopy photosynthetic nitrogen-use efficiency: Evidence from late-sown winter wheat. Environmental and Experimental Botany, **159**: 75-86.

Zhao Y.T., Ali A., Yan E.R. (2017). The plant economics spectrum is structured by leaf habits and growth forms across subtropical species. Tree Physiology, **37**: 173-185.

Zhu S.D., Li R.H., Song J., He P.C., Liu H., Berninger F., Ye Q. (2016). Different leaf cost-benefit strategies of ferns distributed in contrasting light habitats of sub-tropical forests. Annals of Botany, **117**: 497-506.